STUDIA UBB CHEMIA, LXXI, 2, 2026 (p. 171-187)
(RECOMMENDED CITATION)
DOI:10.24193/subbchem.2026.2.09

EFFECT OF TRACE SILICON ON THE PROPERTIES OF IRON-BASED HETEROGENEOUS FENTON CATALYSTS

Jianjun ZHAO[a,*], Yan SHU[a], Leifeng JIA[b], Xianfeng ZHANG[a], Muxin LIU[a], Xu LI[a], Anping XU[a], Xiaoxuan ZHANG[a], Jing YE[a], Ran RONG[a], Jiatong HAN[a], Shenghao LIAO[a]

ABSTRACT. It is an important task for modifying heterogeneous Fenton catalysts to effectively degrade organic pollutants in water. Most studies have modified heterogeneous Fenton catalysts through addition of other metal active species. Here, a series of Si-Fe/γ-Al_2O_3 (x, x = Si/Fe mass ratio per gram of support) catalysts were prepared via wet impregnation method, and the characterization results show that the addition of trace Si (x < 0.10) facilitated the dispersion of Fe species, thereby leading to an increase in the specific surface area, average pore size and pore volume of the catalysts. At the same time, trace Si addition can effectively improve the acid-base properties of the catalyst surface. All these changes may be beneficial to the catalytic degradation of the phenol simulated wastewater.

Keywords: *heterogeneous Fenton catalyst, trace Si modification, highly dispersed active components, acid-base properties of catalyst.*

INTRODUCTION

In recent decades, the intensification of human activities has led to the increase in the accumulation of organic pollutants in water bodies. Organic pollutants in water are not only harmful to the health of humans and aquatic organisms, but also pose significant environmental risks. These organic pollutants must be treated before they are discharged into natural water bodies [1-4].

[a] *Bengbu University, School of Materials and Chemical Engineering, Bengbu, 233030 China.*
[b] *General Water of China (Bengbu) Co., LTD, Bengbu, 233000 China.*
* *Corresponding author: zjj@bbc.edu.cn*

For treating organic wastewater, advanced oxidation processes (AOPs) are considered a promising method because they can convert a variety of organic pollutants into harmless or biodegradable substances [5-8]. In the AOPs, the Fenton reagent, which is composed of iron (or other transition metals) ions and hydrogen peroxide (H_2O_2), has attracted a great deal of researchers' interest [6, 9-11]. The Fenton oxidation process involves the activation of H_2O_2 by Fe^{2+} to generate various reactive oxygen species, such as hydroxyl radicals (•OH), hydrogen peroxide radicals (HO_2•) (equations 1 and 2) [12-15].

$$S\text{-}Fe^{3+} + H_2O_2 \rightarrow S\text{-}Fe^{2+} + HO_2\bullet + H^+ \quad (1)$$

$$S\text{-}Fe^{2+} + H_2O_2 + H^+ \rightarrow S\text{-}Fe^{3+} + H_2O + \bullet OH \quad (2)$$

where S represents the catalyst surface.

With a high redox potential of 2.8 V, the •OH can effectively degrade most organic pollutants into small molecules (such as CO_2 and H_2O) or biodegradable compounds in a non-selective manner. The HO_2• with a slightly weaker oxidation ability (redox potential of 1.50 V) can also participate in the degradation of pollutants (equations 3 and 4) [14].

$$\bullet OH + \text{organics} \rightarrow \ldots\ldots \rightarrow CO_2 + H_2O \quad (3)$$

$$HO_2\bullet + \text{organics} \rightarrow \text{by products} \quad (4)$$

The degradation of organic wastewater using the Fenton reagent includes the homogeneous Fenton process and the heterogeneous Fenton process. Compared with the homogeneous Fenton process, the heterogeneous Fenton process has attracted much attention because of its easy separation of catalyst and avoiding secondary pollution to water bodies [11, 16-18].

Improving the activity of heterogeneous Fenton catalysts is a critical technology in the field of organic wastewater degradation. In order to improve the efficiency of heterogeneous Fenton catalysts, external energies such as ultraviolet lights, ultrasonic waves and microwaves are often used in the catalytic system. Although these methods effectively improve catalyst activity, the high cost of external energy hinders the practical application of these methods [19]. Therefore, fabricating a catalyst with higher activity that requires no external energy supply is one of the goals of researchers devoted to heterogeneous Fenton catalysts.

The modification of heterogeneous Fenton catalysts remains a key focus in contemporary catalysis research. Dopants such as graphene, activated carbon (AC), boron (B), nitrogen (N), sulfur (S), and phosphorus (P) can effectively modulate electron transfer during the catalytic process, thereby enhancing catalytic activity [20-22]. However, an undeniable fact is that the highly dispersed active components can not only improve the microstructure

of the catalyst, but also optimize its surface properties, thereby further enhancing the catalyst activity. Thus, the development of catalysts with highly dispersed active components is an important aspect of research on heterogeneous Fenton catalytic system [19, 23, 24].

Currently, silicon (Si) has been employed in iron-based Fenton catalysts primarily as a high-content support material (e.g., silica or mesoporous silica) [25, 26] or a physical coating shell to suppress metal leaching [27-29], rather than as a trace dopant for interface regulation. Recent studies involving Si-Fe systems, such as Fe on silica support or core-shell structured SiO_2 coating, focus on bulk structural effects rather than atomic-scale control of the Fe–support interface [25-27, 29]. To date, no literature has documented the influence of trace Si on the performance of Fe-based heterogeneous Fenton catalysts (with Si/Fe mass ratio < 0.1) and the corresponding mechanism.

In this work, a series of Si-Fe/γ-Al_2O_3 (x, x = Si/Fe mass ratio per gram of support) catalysts were prepared and used for the degradation of phenol simulated wastewater. The innovation of this study is reflected in the following aspects: In the Si-Fe/γ-Al_2O_3 (x < 0.10), the introduction of Si elements can effectively enhance the dispersion of the active component Fe, increase the specific surface area of the catalyst, optimize its pore structure, and regulate the acid-base properties of the catalyst surface. Consequently, the catalytic activity of the catalyst is significantly improved. The main objectives include: (1) Structure, morphology and chemical properties of Si-Fe/γ-Al_2O_3 (x) catalysts were analyzed by various characterization methods; (2) Catalytic activity of Si-Fe/γ-Al_2O_3 (x) catalysts for the degradation of phenol simulated wastewater was investigated; (3) Hypothetical catalytic mechanism of Si-Fe/γ-Al_2O_3 (x) catalysts for the degradation of organic wastewater was deduced.

RESULTS AND DISCUSSION

Catalyst Characterization

The XRD patterns of the as prepared Si-Fe/γ-Al_2O_3 (x) catalysts are presented in Figure 1a. For all the samples, there are no strong diffraction peaks which indicate that the prepared catalysts show high dispersion states or amorphous structure. However, there are clear diffraction peaks at 37.4°, 45.8° and 67.3° which are assigned to the (311), (400) and (440) crystallographic faces of γ-Al_2O_3 respectively [PDF no. 10-0425]. Meanwhile, for all the Si-Fe/γ-Al_2O_3 (x) samples, there are weak diffraction peaks (α and b peaks) at 33.2°, 35.6° which are assigned to the (104) and (110) crystallographic faces of α-Fe_2O_3 (PDF no. 33-0664).

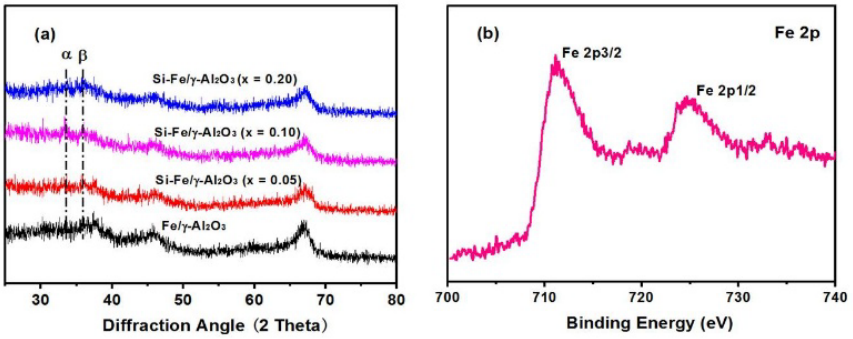

Figure 1. (a) XRD patterns of Si-Fe/γ-Al_2O_3 (x) catalysts and (b) Fe 2p XPS spectra of a Si-Fe/γ-Al_2O_3 (x = 0.10) sample.

In order to further verify the valence state of Fe element in the catalysts, XPS measurement is employed to determine the valence state of Fe on the surface of the Si-Fe/γ-Al_2O_3 (x = 0.10) sample, and the results are shown in Figure 1b. Two distinct peaks at binding energies of 711.1 eV for Fe 2p3/2 and 724.4 eV for Fe 2p1/2 with a weak satellite peak at 718.8 eV are observed, which further indicates that Fe in the Si-Fe/γ-Al_2O_3 (x = 0.10) sample is mainly in the +3 valence [30, 31].

The crystallite size of α-Fe_2O_3 in the Si-Fe/γ-Al_2O_3 (x) catalysts is calculated using the Scherrer equation 5:

$$D = k\lambda/\beta\cos\theta \quad (5)$$

where D represents the crystallite size, k denotes the shape factor (taken as 0.89), λ is the X ray wavelength (Cu Kα radiation, λ = 0.1542 nm), β is the full width at half maximum (FWHM) of the diffraction peak, and θ corresponds to the angular position of the peak maximum. The calculation is applied to the (110) diffraction peak of α-Fe_2O_3, and the results are shown in Table 1.

Table 1. Crystallite size of α-Fe_2O_3 in the Si-Fe/γ-Al_2O_3 (x) catalysts.

Catalyst	FWHM	crystallite size (nm)
Fe/γ-Al_2O_3 (x = 0)	0.168	0.8581
Si-Fe/γ-Al_2O_3 (x = 0.05)	0.187	0.7709
Si-Fe/γ-Al_2O_3 (x = 0.10)	0.273	0.5280
Si-Fe/γ-Al_2O_3 (x = 0.20)	0.148	0.9740

Table 1 shows that adding a small amount of Si doping to the Fe/γ-Al_2O_3 catalyst (x < 0.10) leads to a gradual reduction in the crystallite size of α-Fe_2O_3, which decreases from 0.8581 nm to 0.5280 nm. However, at x = 0.2, the α-Fe_2O_3 crystallite size increases, reaching 0.9740 nm.

N_2 adsorption-desorption measurements are carried out to evaluate the specific surface area (BET surface area) and pore size distribution of the prepared catalysts. The BET surface areas of the Fe/γ-Al_2O_3 (x = 0), Si-Fe/γ-Al_2O_3 (x = 0.05), Si-Fe/γ-Al_2O_3 (x = 0.10) and Si-Fe/γ-Al_2O_3 (x = 0.20) samples are determined to be 255.96, 249.72, 275.82, and 257.84 $m^2 \bullet g^{-1}$, respectively (Table 2). It can be inferred that the addition of a small amount of Si (x < 0.10) is conducive to the increase of specific surface area of the Fe/γ-Al_2O_3 catalyst, and the increase of the catalyst's specific surface area in a certain range is helpful to improve the catalyst's activity. It can also be seen from Table 2 that the pore volume and average pore diameter of the Si-Fe/γ-Al_2O_3 (x = 0.10) catalyst are larger than those of the other catalysts. The larger pore volume and average pore diameter help to reduce the steric hindrance in the reaction, thereby improving the catalyst's activity.

Table 2. BET surface area, average pore diameters and pore volume for the Si-Fe/γ-Al_2O_3 (x) catalysts.

Catalyst	BET surface area ($m^2 \cdot g^{-1}$)	verage pore diameter (nm)	Pore volume ($mL \cdot g^{-1}$)
Si-Fe/γ-Al_2O_3 (x = 0)	255.96	4.56	0.389
Si-Fe/γ-Al_2O_3 (x=0.05)	249.72	4.60	0.375
Si-Fe/γ-Al_2O_3 (x=0.10)	275.82	4.68	0.391
Si-Fe/γ-Al_2O_3 (x=0.20)	257.84	4.63	0.376

Figure 2 shows the N_2 adsorption-desorption isotherms of the Si-Fe/γ-Al_2O_3 (x) catalysts as well as the corresponding pore size distribution. All samples exhibit type IV adsorption-desorption isotherms, which indicates the existence of mesopores in the catalysts (Figure 2a) [31]. Interestingly, Figure 2b shows that the Si-Fe/γ-Al_2O_3 (x = 0.10) sample has a more concentrated pore size distribution than the other samples, although this catalyst has the largest specific surface area. It is reasonable to infer that the Si-Fe/γ-Al_2O_3 (x = 0.10) catalyst with larger specific surface area, pore volume and pore size has better catalytic activity than the other catalysts.

The surface morphology and the corresponding Fe dispersion of the Si-Fe/γ-Al_2O_3 (x) catalyst samples were observed via SEM and EDS. As shown in Figure 3, the surface morphology of the Fe/γ-Al_2O_3 (x = 0) catalyst was relatively smooth, and a few crystal particles were present on its surface. With the increase of Si in the catalyst, more dispersed particles appeared on the catalyst surface (x = 0.05 and 0.1). Meanwhile, the Si-Fe/γ-Al_2O_3 (x = 0.1) catalyst exhibited relatively uniform particle dispersion on its surface. While the mass ratio of Si to Fe was 0.2 in the catalyst, the particles on the catalyst surface began to grow larger. This phenomenon shows that the addition of a

small amount of Si (x < 0.1) in the catalyst contributes to the dispersion of particles on the catalyst surface. Notably, agglomeration of surface particles occurs when the Si content exceeds 0.1. This observation correlates well with the increase in crystallite size estimated by the Scherrer equation.

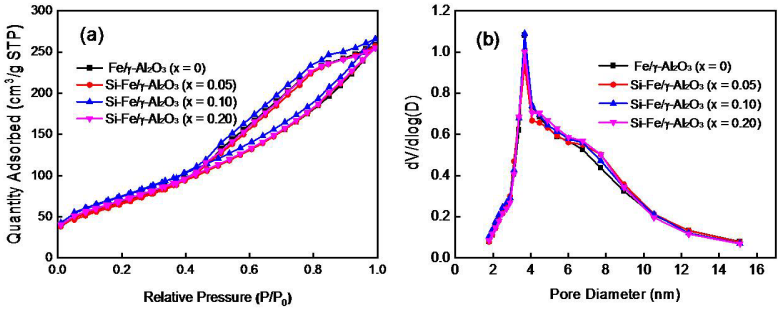

Figure 2. (a) N_2 adsorption-desorption curves and (b) pore diameter distribution of the Si-Fe/γ-Al_2O_3 (x) catalysts.

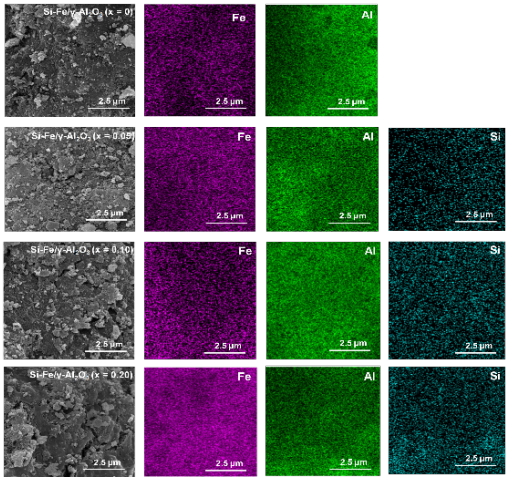

Figure 3. SEM images of Si-Fe/γ-Al_2O_3 (x) catalysts and corresponding Fe, Al, Si elemental mapping (left-right).

As can be seen in Figure 3 the Fe was increasingly evenly dispersed on the catalyst surface with the increase of Si content (x < 0.1) in the catalyst. The possible reasons for this phenomenon are as follows. When a certain amount of TEOS is added to ferric nitrate solution, Si-OH compounds were produced by hydrolysis to different degrees, the corresponding hydrolysis reaction is presented in equation 6.

$$Si(OC_2H_5)_4 + 4H_2O \rightarrow Si(OH)_4 + 4C_2H_5OH \quad (6)$$

The Si-OH in the resulting compound acts as a bridge, connecting the Fe^{3+} in the solution to the support. When the Si content is low (x = 0.05, 0.1), a small amount of silicic acid preferentially reacts with the hydroxyl groups on the surface of AlO(OH) to form a Si-O-Al interface bonding structure; at the same time, silicic acid undergoes coordination interaction with Fe^{3+}, stabilizing and anchoring the Fe ions on the surface of the support, which led to a more uniform distribution of the active component Fe on the surface of the support, as shown in reaction equations 7 and 8.

$$Si(OH)_4 + Al\text{-}OH(surface) \rightarrow Al\text{-}O\text{-}Si(OH)_3 + H_2O \quad (7)$$

$$Fe^{3+} + Al\text{-}O\text{-}Si(OH)_3 \rightleftharpoons Al\text{-}O\text{-}Si(OH)_2\text{-}O\text{-}Fe^{2+} + H^+ \quad (8)$$

When the Si content is high (x = 0.2), silicic acid formed by excessive hydrolysis of TEOS undergoes intermolecular condensation on the Boehmite support surface, producing a continuous amorphous SiO_2 coating. This coating shields the hydroxyl groups on the support surface and weakens the strong metal–support interaction between Fe and the support, further leading to agglomeration of the active components on the catalyst surface, as shown in reaction equation 9.

$$nSi(OH)_4 \rightarrow (SiO_2)n + 2nH_2O \quad (9)$$

As a result, Fe was more evenly distributed on the surface of Si-Fe/γ-Al_2O_3 (x = 0.10) catalyst. Xiao et al [32] found that the volume percentages of blocky-shaped phases increased with increasing addition of Si (0.10 - 0.20 wt.% Si). This phenomenon is consistent with the results of this study.

Figure 4 shows a typical SEM image and EDS spectra of the Si-Fe/γ-Al_2O_3 (x = 0.10) catalyst sample in the specified region. The presence of C in the EDS spectra is due to the addition of TEOS in the catalyst preparation, and the peaks at 2.120 and 9.712 keV (Figure 4b) belong to Au, which is mentioned in the “EXPERIMENTAL SECTION”. The corresponding elemental compositions of the Si-Fe/γ-Al_2O_3 (x = 0.10) catalyst sample are depicted in Table 3. It can be seen that the mass ratio of Si to Fe in the specific portion of the catalyst is 1.25 : 12.40, which is approximately equal to the theoretical value of 0.1. This phenomenon indicates that Si and Fe are well distributed on the surface of the Si-Fe/γ-Al_2O_3 (x = 0.10) catalyst in the specific portion; i.e., the active component Fe is fully exposed on the catalyst surface, which is favorable to the catalytic reaction.

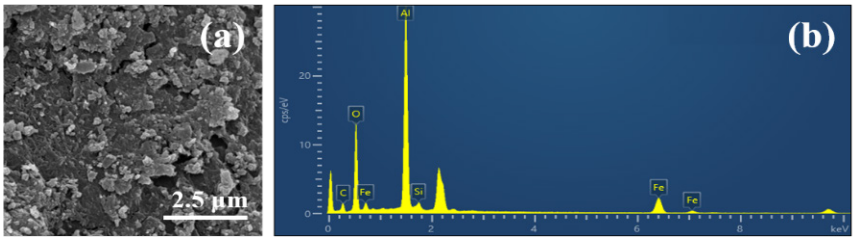

Figure 4. SEM image (a) and EDS spectra (b) of Si-Fe/γ-Al_2O_3 (x = 0.10) catalyst.

Table 3. Elemental composition of Si-Fe/γ-Al_2O_3 (x = 0.10) catalyst in the specified region.

Elements	wt.%
C	14.88
O	37.92
Al	33.54
Si	1.25
Fe	12.40
Total	100.00

The acid-base properties of heterogeneous catalysts are an important factor affecting the activity of catalysts [33]. Temperature programmed desorption (TPD) is an important method to characterize the acid-base properties of catalysts. CO_2-TPD analyses of the Si-Fe/γ-Al_2O_3 (x) catalysts were determined, and the results are shown in Figure 5. Accordingly, two peaks at 340 °C and 601 °C were observed in all samples, indicating the presence of two distinct types of alkaline sites in the catalysts. It can be seen that the Si-Fe/γ-Al_2O_3 (x = 0) catalyst exhibits a relatively high content of both types of alkaline sites. However, the introduction of a small amount of Si into the Fe/γ-Al_2O_3 catalyst (x = 0) resulted in a slight decrease in the content of these two alkaline sites in the resulting catalyst.

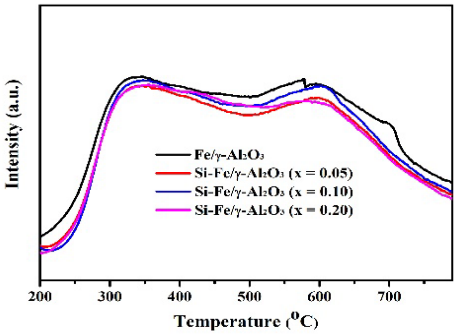

Figure 5. CO_2-TPD profiles of the Si-Fe/γ-Al_2O_3 (x) catalysts.

The reasons for this phenomenon are as follows: For the Fe/γ-Al_2O_3 catalyst, its basicity mainly originates from the interaction between coordinatively unsaturated Al^{3+} on the catalyst surface and O^{2-}, which gives rise to alkaline sites (Al-O^-). When a small amount of Si is introduced into the catalyst, Si-O-Al bonds are formed on the surface, which directly consume the Al-O^- basic sites and generate Si-O-Al bridges, thus further reducing the number of alkaline sites. The corresponding reaction is depicted in equation 10.

$$\equiv Al\text{-}O^- + \equiv Si\text{-}OH \rightarrow \equiv Al\text{-}O\text{-}Si\equiv + OH^- \quad (10)$$

Catalytic Performance

Phenol, being a type of organic pollutant that is the hard to degrade, how to completely decompose it into environmentally harmless small molecules has become a focus of research [24, 31, 34-36]. At the same time, as an important parameter to describe the content of organic pollutants in wastewater, Chemical Oxygen Demand (COD) is used as a key index to evaluate water pollution in many countries and regions. COD removal rate refers to the degree of oxidation of organic pollutants in wastewater, or more specifically, the process by which larger molecules are broken down into smaller fragments to the maximum extent (i.e., mineralization into CO_2 and H_2O) [24, 31, 35]. In this study, the COD removal rate was used as an evaluation index for catalyst activity.

The catalytic activities of the Si-Fe/γ-Al_2O_3 (x) catalysts were evaluated by the degradation of the 100 mg•L^{-1} phenol simulated wastewater under the optimal reaction conditions reported in our previous study [24]. Specifically, the reaction temperature was 30 ^oC, the initial pH of the wastewater was 3.5, the dosage of H_2O_2 was 1.5 mL, and the reaction time was 60 minutes.

Figure 6 shows the effects of different Si-Fe/γ-Al_2O_3 (x) catalysts on the COD removal rate of phenol simulated wastewater. It is observed that the COD removal rate of the phenol simulated wastewater was approximately 66% when the Fe/γ-Al_2O_3 (x = 0) catalyst was used. With the increase in Si content in the Si-Fe/γ-Al_2O_3 (x < 0.1) catalyst, the COD removal rate of the phenol simulated wastewater increased. For the Si-Fe/γ-Al_2O_3 (x = 0.10) catalyst, the highest COD removal rate (83%) was achieved under the given reaction conditions. Subsequently, with the further increase in Si content in the catalysts, the catalytic degradation for phenol simulated wastewater decreased. The possible reasons for this phenomenon are discussed in the “Catalytic Mechanism” section of this study.

Figure 6 demonstrates that the Si-Fe/γ-Al_2O_3 (x = 0.1) catalyst exhibits outstanding catalytic activity, and characterization of its physical and chemical properties further confirms its excellent intrinsic structural stability.

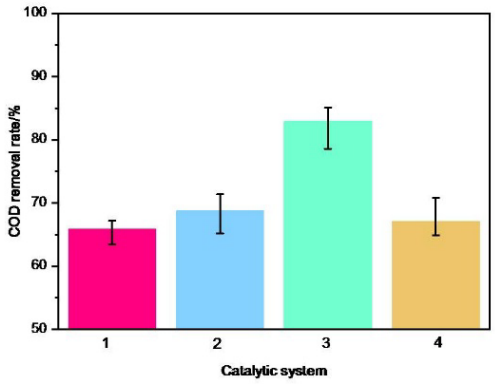

Figure 6. Influence of different catalysts on COD removal rate of phenol simulation wastewater. (1) Fe/γ-Al_2O_3 (x = 0); (2) Si-Fe/γ-Al_2O_3 (x = 0.05); (3) Si-Fe/γ-Al_2O_3 (x = 0.10); (4) Si-Fe/γ-Al_2O_3 (x = 0.20).

XRD results reveal a well-defined γ-Al_2O_3 crystal phase, indicating that trace Si doping does not damage the support lattice structure. SEM-EDS elemental mapping further verifies the uniform distribution of Fe elements within the catalyst. Additionally, BET results show that trace Si modification optimizes the catalyst's pore structure (including specific surface area, pore volume, and average pore size) while preserving good structural integrity. This intrinsic structural stability, attributed to trace Si doping, is a key advantage that facilitates maintaining the catalyst's structural and catalytic performance during the reaction process.

Catalytic Mechanism

To explore the correlation between the catalytic activity of catalysts in degrading the phenol simulated wastewater and their characterization results, this paper proposes a hypothetical catalytic reaction mechanism. In this study, the addition of the trace Si element during the catalyst preparation process may affect not only the physical properties of the prepared catalysts but also their chemical properties.

The following is a hypothetical catalytic reaction mechanism proposed based on the changes in physicochemical properties and reaction behaviors observed over Si-Fe/γ-Al_2O_3 (x) catalysts with the introduction of trace Si. The proposed mechanism is based on existing literature and has not yet been verified by direct experimental evidence such as radical scavenging experiments in this study.

On the one hand, the physical properties of catalysts may affect their catalytic activity. According to the XRD and XPS characterization results of the Si-Fe/γ-Al_2O_3 (x) catalysts, the Fe element in the catalysts exists in the form of α-Fe_2O_3. Meanwhile, the XRD, SEM, and EDS results showed that the addition of a small amount of Si in Si-Fe/γ-Al_2O_3 (x) promoted the distribution of Fe species, which further led to changes in the specific surface area, average pore size and pore volume of the catalysts (as shown by the N_2 adsorption-desorption results). These changes may be conducive to the catalytic degradation of phenol simulated wastewater. Firstly, the highly dispersed active component Fe in the catalyst is more favorable to react with H_2O_2 in the reaction system to produce highly oxidizing •OH (equations 1 and 2), thereby further promoting the degradation of phenol (equation 3). Secondly, the increase in the specific surface area of the catalyst expands the reaction region, thereby improving the phenol degradation efficiency. Thirdly, the increase in pore volume reduces reaction hindrance, which further enhances the degradation efficiency of phenol simulated wastewater. The effect of adding a trace amount of Si ($x < 0.10$) on the physical properties of the catalyst, as well as the subsequently inferred influence on its catalytic activity, are illustrated in Scheme 1.

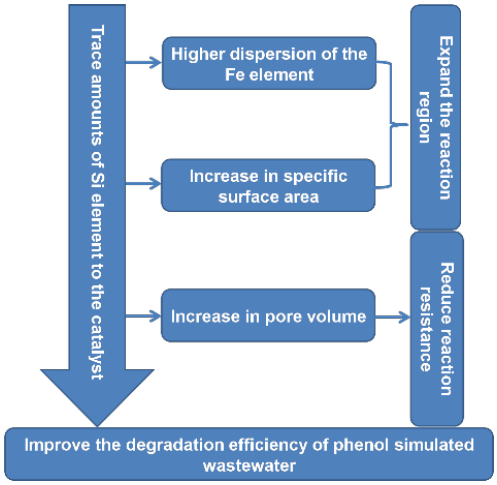

Scheme 1. The influence of trace Si doping on the physical properties and phenol wastewater degradation performance of the Si-Fe/γ-Al_2O_3 ($x < 0.10$) catalyst.

On the other hand, the chemical properties of catalysts may also influence their catalytic activity. In heterogeneous catalytic reactions, the adsorption of reactants on the catalyst surface is generally considered to be

the first step of heterogeneous catalysis [37, 38]. A non-linear relationship may exist between the number of alkaline sites on the catalyst surface and the catalytic activity, and surface alkaline sites may play a key role in balancing these factors. For instance, an excessive number of alkaline sites inhibit the Fe^{3+}/Fe^{2+} redox cycle in the Fenton reaction (which generates highly oxidative •OH, as shown in equations 1 and 2). Conversely, an insufficient number of alkaline sites will decrease the adsorption capacity toward phenolic pollutants, since phenolic compounds in wastewater are acidic. The competitive balance between these two effects may jointly determine the degradation efficiency.

Overall, the number of alkaline sites in the Si-Fe/γ-Al_2O_3 (x) catalysts may affect the COD removal rate of phenolic wastewater by regulating two key aspects: pollutant adsorption capacity and active species (•OH) generation efficiency. Only when the number of alkaline sites is within a suitable range can the synergistic effect between adsorption and the generation of •OH to achieve the optimal COD removal performance; otherwise, a decline in COD removal rate will occur.

It is speculated that the Si-Fe/γ-Al_2O_3 (x = 0.1) catalyst has an appropriate number of surface alkaline sites, which not only allows efficient adsorption of phenolic pollutants but also promotes the generation of strong oxidizing species such as •OH (equations 1 and 2), thus achieving the highest COD removal rate. In this study, Scheme 2 illustrates the effect of the number of alkaline sites on the degradation performance of Si-Fe/γ-Al_2O_3 (x) catalysts for phenol simulated wastewater.

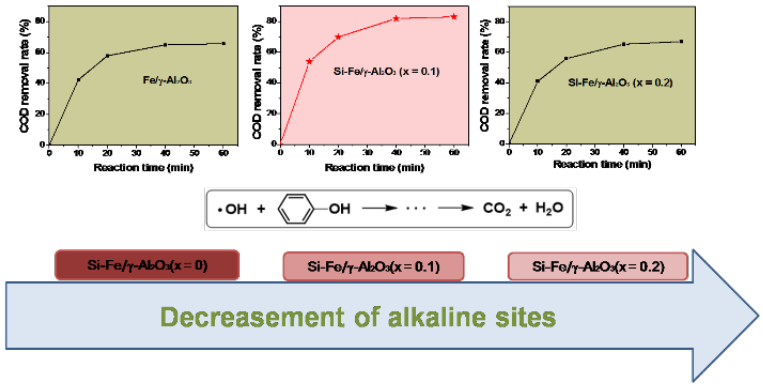

Scheme 2. Effect of surface alkaline sites of the Si-Fe/γ-Al_2O_3 (x) catalysts on degradation performance of phenol simulated wastewater.

The limitations of this study are as follows: it only focused on the influence of trace Si elements on the activity of iron-based catalysts. Specifically, the addition of trace Si elements in the catalyst was found to significantly enhance its catalytic activity. However, the changes in the service life of the catalyst before and after modification and the influencing factors still remain to be further explored. Meanwhile, the impact of Si on other active components (such as copper, manganese, etc.) also needs in-depth investigation, which will be one of the key focuses of subsequent research.

Looking ahead, this research not only offers a feasible strategy for the preparation of catalysts with highly dispersed active components, but also establishes a theoretical basis for the efficient application of such catalysts in the degradation of organic wastewater.

CONCLUSIONS

In the Si-Fe/γ-Al_2O_3 (x) catalysts prepared by the impregnation method, the mass ratio of Si to Fe enables us to gain a deep understanding of the influence of trace Si on the physical and chemical properties of the catalysts, and subsequently on the catalyst's activity in degrading phenolic wastewater. When a small amount of Si is added to a Fe/γ-Al_2O_3 catalyst, the dispersion of the active component Fe on the catalyst surface is enhanced, and the specific surface area, average pore size, and pore volume of the Si-Fe/γ-Al_2O_3 catalysts ($x < 0.1$) increase. Meanwhile, the introduction of a small amount of Si can also improve the alkaline sites on the catalyst surface, which is beneficial for enhancing the catalytic activity. As a result, the Si-Fe/γ-Al_2O_3 ($x = 0.1$) catalyst demonstrated outstanding catalytic activity in the degradation of phenolic wastewater. Under the given conditions, the COD removal rate of the phenolic wastewater by this catalyst reached 83%, which was superior to the activity of other catalysts. This study proposes a novel and effective strategy for preparing heterogeneous catalysts with highly dispersed active components, and also enables the improvement of the surface acid-base properties of such catalysts.

EXPERIMENTAL SECTION

Materials And Reagents

Analytical grade ferric nitrate ($Fe(NO_3)_3•9H_2O$), analytical grade phenol, sulfuric acid (H_2SO_4), potassium dichromate ($K_2Cr_2O_7$), silver sulfate (Ag_2SO_4), hydrogen peroxide (H_2O_2, 30%), and tetraethyl orthosilicate ($Si(OC_2H_5)_4$, TEOS,

>99%) were purchased from Sinopharm Chemical Reagent Co., Ltd. Analytical grade Boehmite was provided by Zibo Hengqi Powdered Advanced Material Co., Ltd, China. Above reagents were used as received without further purification.

Catalyst Preparation

A series of Si-Fe/γ-Al_2O_3 (x) catalysts were prepared by an impregnation method, where x represents the mass ratio of Si to Fe per gram of support.

First, an impregnation solution was prepared. 14.4284 g of $Fe(NO_3)_3$•$9H_2O$ was dissolved in 16 mL of deionized water under stirring until completely dissolved, and the resulting solution was equally divided into four portions. Then, 0, 0.2019, 0.4038, and 0.8076 mL of TEOS solution were added to these four solutions, respectively.

Next, 5.0 g of Boehmite with a particle size of 0.250-0.425 mm (40 - 60 mesh) was added into each solution, and the mixtures were stirred continuously at room temperature for 12 h.

Subsequently, the mixtures were dried in a constant temperature drying oven at 120 °C. The dried samples were transferred to a crucible and calcined in a Muffle oven at 500 °C for 4 h.

After cooling naturally to room temperature, in this paper, the final catalyst is labeled as Si-Fe/γ-Al_2O_3 (x), where x = 0, 0.05, 0.1, and 0.2, corresponding to the theoretical mass ratio of Si to Fe. The theoretical Fe content of all catalysts is 0.1 grams of Fe per gram of support.

Catalyst Characterization

Powder X-ray diffraction (XRD) patterns were collected on a Rigaku D/max-RA X-ray diffractometer with Cu Ka radiation, operating at a respective voltage of 40 kV and current of 40 mA. Diffractograms were recorded in the 2θ range of 20–80°.

X-ray photoelectron spectroscopy (XPS) data were collected on a Thermo Scientific K-Alpha instrument using monochromic Al Kα radiation. The binding energies were referenced to the C 1s line at 284.8 eV from adventitious carbon.

The surface area and the porous structure were characterized by N_2-physisorption at 77 K using a Micromeritics Tristar II 3020 surface analyzer. Prior to measurement, samples were degassed at 350 °C for 4 h. Specific surface areas were calculated using the Brunauer-Emmett-Teller (BET) equation at $P/P_0 < 0.3$. Pore size distributions were determined from the desorption branch of the N_2 adsorption isotherm using the Barrett-Joyner-Halenda (BJH) method.

The morphology and microstructure of the as-prepared catalysts were observed using a Zeiss Supra 40 scanning electron microscope (SEM, Germany). Prior to imaging, the samples were sprayed with gold to enhance conductivity, and then were examined under high vacuum at an accelerating voltage of 20 kV. Chemical composition and semi-quantitative elemental analysis were performed simultaneously using an Oxford Instruments X-Max energy dispersive spectrometer (EDS).

Carbon dioxide temperature programmed desorption (CO_2-TPD) was carried out on a laboratory-made apparatus to investigate the surface acid-base properties of Si-Fe/γ-Al_2O_3 (x) catalysts. 50 mg of sample were loaded in a quartz tubular reactor (i.d.: 6 mm) prior to the measurement, and then they were heated to 500 ^oC at the rate of 10 ^oC/min under a He flow, followed by being maintained at 500 ^oC for 1 h. After natural cooling to room temperature, pulse CO_2 gas into the catalyst until adsorption saturation. The physically adsorbed CO_2 was removed under a He flow at 100 ^oC for 1 h. Then, the sample was heated to 800 ^oC at a rate of 10 ^oC/min. The desorbed CO_2 was analyzed by an online gas chromatograph with a TCD detector.

Catalytic Activity Measurements

The catalytic activities of Si-Fe/γ-Al_2O_3 (x) samples were evaluated by the degradation of phenol simulated wastewater. The optimum experimental conditions were employed according to our previous work [24]. The catalytic degradation of phenol simulated wastewater was tested in a 150 mL three necked glass flasks at 30 ^oC. Firstly, the initial pH of phenol simulated wastewater with a concentration of 100 mg•L^{-1} was adjusted to 3.5 with a dilute H_2SO_4 solution, and its corresponding COD was about 238 mg•L^{-1}. Then, 50 mL phenol simulated wastewater, 150 mg catalyst, and 1.5 mL 30% (wt.%) aqueous H_2O_2 solution were added to a three necked glass flask, and the mixture was stirred constantly to ensure good dispersion of the catalyst in the reaction system at 30 °C. After a 60 min reaction, a 20 mL sample was extracted from the reaction system to determine its COD value, which was measured by the standard $Cr_2O_7^{2-}/Cr^{3+}$ method.

For each COD value, parallel experiments were conducted under identical experimental conditions, with a minimum of three repetitions. After the experiments are completed, the average value of the results from each experimental group shall be used as the final data.

The COD removal rate of the wastewater was calculated using equation 11:

$$\text{COD removal rate (\%)} = (COD_B\text{-}COD_A)/COD_B \times 100 \quad (11)$$

In the above equation, COD_B denotes the initial COD value of the wastewater, while COD_A represents its COD value after degradation.

ACKNOWLEDGMENTS

This research was funded by the Anhui Province Quality Engineering Project (2020kcszjxtd52); the National Natural Science Foundation of China (21978003); the National Natural Science Foundation of China (21503004); the Anhui Province Discipline (Specialty) Leader Cultivation Project (DTR2024050); the Guidance project of Science and Technology Innovation of Bengbu (20210349); Bengbu University Application-level Scientific Research Project (2024YYX30pj); the Bengbu University Student Innovation and Entrepreneurship Project (202511305007, S202511305015); the Cultivation Program for the Outstanding Young Teachers of Anhui Province (YQZD2023082) and the Bengbu University Research Team Fund (BBXYKYTDxj09).

REFERENCES

1. V. Vinayagam; K. N. Palani; S. Ganesh; S. Rajesh; V. V. Akula; R. Avoodaiappan; O. S. Kushwaha; A. Pugazhendhi; *Environ. Res.*, **2024**, 240, 117500.
2. K. M. AlAqad; M. M. Abdelnaby; A. Tanimu; I. Abdulazeez; A. M. Elsharif; *Environ. Pollut. Manag.*, **2025**, 2, 1-13.
3. T. Weng; H. Du; H. Luo; M. Jiang; Z. Chen; J. Wang; H. Chen; *Sep. Purif. Technol.*, **2025**, 355, 129573.
4. K. Haarstad; H. J. Bavor; T. Mæhlum; *Water Sci. Technol.,* **2012**, 65, 76–99.
5. B. Tunçsiper; *J. Clean. Prod.,* **2019**, 04, 211.
6. S. Yang; S. Yu; Y. Dong; J. Liu; P. Zhou; H. Zhang; Z. Xiong; C. S. He; B. Lai; *J. Hazard. Mater.*, **2025**, 490, 137752.
7. P. Koundle; N. Nirmalkar; G. Boczkaj; *J. Environ. Manage.*, **2025**, 374, 124107.
8. K. Tian; L. Hu; L. Li; Q. Zheng; Y. Xin; G. Zhang; *Chinese Chem. Lett.*, **2022**, 33, 4461-4477.
9. J. Nie; Z. Li; W. Liu; Z. Sang; D. A. Yang; L. Wang; F. Hou; J. Liang; *Adv. Mater.*, **2025**, 37, 2420236.
10. D. Ma; H. Yi; C. Lai; X. Liu; X. Huo; Z. An; L. Li; Y. Fu; B. Li; M. Zhang; L. Qin; S. Liu; L. Yang; *Chemosphere*, **2021**, 275, 130104.
11. X. Zou; Q. Shi; M. Cheng; D. Huang; G. Zhang; W. Wang; G. Wang; H. Liu; Y. Chen; A. Chen; S. Deng; *Adv. Energy Mater.*, **2025**, 15, 2501424.
12. R. Lin; Y. Li; T. Yong; W. Cao; J. Wu; Y. Shen; *J. Environ. Manage.*, **2022**, 306, 114460.
13. F. N. Chergui; S. Ounoki; M. Chebbi; T. Masmoudi; Y. Kadmi; *Int. J. Environ. Sci. Te.*, **2025**, 22, 13717–13730.
14. Y. Zhu; R. Zhu; Y. Xi; J. Zhu; G. Zhu; H. He; *Appl. Catal. B: Environ.*, **2019**, 255, 117739.

15. H. Liu; S. Tang; Z. Wang; Q. Zhang; D. Yuan; *Chemosphere*, **2024**, 353, 141581.
16. M. Zhang; H. Dong; L. Zhao; D. Wang; D. Meng; *Sci. Total Environ.*, **2019**, 670, 110-121.
17. J. Cai; J. Xiao; G. Du; Q. An; W. Tong; *J. Mater. Chem. B*, **2025**, 13, 4544-4569.
18. X. Wang; D. Zhang; Y. Cheng; B. Wu; L. Sun; *Molecules*, **2025**, 30, 4549.
19. J. Wang; C. Liu; J. Qi; J. Li; X. Sun; J. Shen; W. Han; L. Wang; *Environ. Pollu.*, **2018**, 243, 1068-1077.
20. L. Ma; Y. Wang; Y. Chen; D. Xu; R. Han; D. Jiao; H. Xing; D. Wang; X. Yang; *ACS Nano.,* **2025**, 19, 28410–28421.
21. P. Compton; N. R. Dehkordi; P. Larese Casanova; A. N. Alshawabkeh; *J. Chem. Eng. Catal.,* **2022**, 1: 203.
22. S. Guo; N. Yuan; G. Zhang; J. C. Yu; *Micropor. Mesopor. Mater.,* **2017**, 238, 62-68.
23. Q. U. Ain; U. Rasheed; Z. Chen; R. He; Z. Tong; *J. Ind. Eng. Chem.*, **2024**, 134, 327-342.
24. J. Zhao; K. Ding; B. Ding; *Water Air Soil Poll.*, **2017**, 228, 442.
25. N. K. Puthenveettil; G. Dražic; A. Pintar; N. N. Tušar; *Catalysts,* **2026**, 16, 34.
26. N. Farhadian; S. Liu; A. Asadi; M. Shahlaei; S. Moradi; *J. Mol. Liq.*, **2021**, 321, 114896.
27. J. Zeng; W. Wang; Y. Du; *Environ. Prog. Sustainable Energy,* **2026**, e70397.
28. S. T. Yang; W. Zhang; J. Xie; R. Liao; X. Zhang; B. Yu; R. Wu; X. Liu; H. Li; Z. Guo; *RSC Adv.,* **2014**, 5, 5337-5345.
29. Y. Chen; S. Zhang; Y. Chen; H. Ding; S. Yao; Y. Tang; Z. Qiu; K. Xu; Y. Hu; H. Pang; *Nano Res.,* **2025**, 18, 94907446.
30. B. Ma; Y. Zha; H. Shi; Y. Qin; M. Zhao; J. Li; S. Wang; B. Yan; B. Zhao; Y. Ma; H. Xie; *Sep. Purif. Technol.*, **2025**, 354, 129086.
31. B. Rezaei; M. Khamforoush; F. Rahmani; *J. Clean. Prod.*, **2025,** 513, 145744.
32. C. Xiao; Y. Han; *Mat. Sci. Eng. A*, **2002**, 323, 58-61.
33. V. Calvino-Casilda; R. Martin-Aranda; I. Sobczak; M. Ziolek; *Appl. Catal. A-Gen.*, **2006**, 303, 121-130.
34. A. Cheng; Y. He; X. Liu; C. He; *J. Environ. Sci.*, **2024**, 136, 390-399.
35. X. Wang; Z. Yang; Y. Jiang; P. Zhao; X. Meng; *Sep. Purif. Technol.*, **2024**, 330, 125267.
36. M. Tian; X. Ren; S. Ding; N. Fu; Y. Wei; Z. Yang; X. Yao; *Environ. Res.*, **2024**, 243, 117848.
37. B. W. Chen; M. Mavrikakis; *Nat. Chem. Eng.*, **2025**, 2, 181-197.
38. M. Yaghi; S. Chidiac; S. Awad; Y. El Rayess; N. Zgheib; *Clean Technol.*, **2025**, 7, 62.